

# CO emission from high redshift

Nickolay Y. Gnedin<sup>1</sup>, Joseph Silk<sup>2</sup>, and Marco Spaans<sup>3</sup>

<sup>1</sup>*Center for Astrophysics and Space Astronomy, University of Colorado, Boulder, CO 80309, USA; gnedin@casa.colorado.edu*

<sup>2</sup>*Astrophysics, Department of Physics, Oxford University, Keble Road, Oxford, OX1 3NP, UK*

<sup>3</sup>*Kapteyn Institute, Groningen, 9700 AV, The Netherlands*

## ABSTRACT

Future observations with ALMA will be able to detect star-forming primordial galaxies, and perhaps even their dwarf spheroidal satellites, in CO emission lines at redshifts approaching 10. These observations will compliment other tools designed to study the dawn of galaxy formation, such as NGST and FIRST.

**Key words:** cosmology: theory – galaxies: evolution – galaxies: starburst – ISM: molecules

## 1 INTRODUCTION

Modern cosmology continues to push the boundaries of the known universe to higher and higher redshifts. We are designing telescopes capable of detecting the very first objects that formed in the universe. The real breakthrough will occur in the next decade: the New Generation Space Telescope (NGST), the The Far IR and Submillimeter Space Telescope (FIRST), and the Atacama Large Millimeter Array (ALMA) will allow us to reach cosmological redshifts in excess of 10. ALMA is especially important, because it can observe CO emission from primordial galaxies redshifted into the millimeter band. Because the Cosmic Microwave Background (CMB) temperature increases toward the past, higher rotational levels of the CO molecule are populated at high redshifts (Silk & Spaans 1997; Sakamoto 1999; Blain et al. 2000), resulting in a large negative K-correction. The effect is so large that a star-forming galaxy will appear equally bright at  $z = 5$  and at  $z = 10$ .

At lower redshift, CO emission from galaxies and quasars has already been detected (Solomon, Downes, & Radford 1992; Barvainis et al. 1994; Omont et al. 1996; Guilloteau et al. 1997; Scoville et al. 1997; Barvainis et al. 1998; Frayer et al. 1998; Downes et al. 1999; Frayer et al. 1999; Andreani et al. 2000; Papadopoulos et al. 2000; Papadopoulos et al. 2001). These results provide information on the kinematics and energetics of the star-forming (molecular) ISM and thereby complement observations of the stellar light component in primordial systems.

In this paper we show that ALMA, with its significantly higher sensitivity, will be able to image primordial galaxies to redshift 10 and even beyond. It is conceivable that it will even be able to detect dwarf spheroidal satellites of primordial galaxies and their tidal tails (which should be in abundance at high redshift, where the merger rate is much higher than in the local universe).

**Table 1.** Simulation Parameters

Run	$N$	Box size	Mass res.	Spatial res.
A	$128^3$	$4h^{-1}$ Mpc	$10^{6.6} M_{\odot}$	$1.0h^{-1}$ kpc
B	$64^3$	$2h^{-1}$ Mpc	$10^{6.6} M_{\odot}$	$1.5h^{-1}$ kpc

## 2 METHOD

### 2.1 Simulations

We use the cosmological simulations of reionization reported in Gnedin (2000). The simulations include 3D radiative transfer (in an approximate implementation) and other physical ingredients required for modeling the process of cosmological reionization.

Two simulations of a representative CDM+ $\Lambda$  cosmological model\* were performed with the parameters specified in Table 1. Both simulations were stopped at  $z = 4$  because at this time the rms density fluctuation in the computational box is about 0.25, and at later times the box ceases to be a representative region of the universe.

The two simulations from Table 1 allow us to investigate the sensitivity of our results to the inevitably missing small-scale and large-scale power. The difference between the two runs can be interpreted as the theoretical uncertainty in our calculations, given a cosmological model. Clearly, our results will be different for different assumptions about cosmological parameters.

### 2.2 Calculating CO emission from early galaxies

The code described in Spaans (1996) and applied as in Silk & Spaans (1997) has been used to rerun the models pre-

\* With the following cosmological parameters:  $\Omega_0 = 0.3$ ,  $\Omega_{\Lambda} = 0.7$ ,  $h = 0.7$ ,  $\Omega_b = 0.04$ ,  $n = 1$ ,  $\sigma_8 = 0.91$ , where the amplitude and the slope of the primordial spectrum are fixed by the COBE and cluster-scale normalizations.

arXiv:astro-ph/0106110v1 6 Jun 2001

sented in (Silk & Spaans 1997) with the latest atomic and molecular collision and chemistry data. These models use the Orion molecular cloud and its so-called bar region as being representative of a region of active star formation. The star formation rate in  $M_{\odot} \text{ yr}^{-1}$  of a fiducial model galaxy is then related to the total number of Orion-like star formation sites through division by the average star formation rate of the Orion region,  $\sim 3 \times 10^{-4} M_{\odot} \text{ yr}^{-1}$  (Hillenbrand 1997). In Silk & Spaans (1997) it has been shown that the CMB becomes an important source of excitation at high redshift because of the fortuitous coincidence between the CO level spacing and the  $1+z$  increase in the CMB temperature. This causes galaxies at  $z = 5$  and  $z = 10$  to be observable at similar flux density levels, provided they in fact are present. It has been assumed that the Orion-like regions responsible for the star formation activity occur throughout the model galaxy, and are not all confined to the inner few 100 pc as in Combes, Maoli, & Omont (1999) This assumption decreases the mean optical depth of the CO lines and is most likely to hold at high ( $z > 3$ ) redshifts, when galaxies are still being built up through mergers and accretion.

In order to compute the spectrum of CO emission as a function of wavelength, for a given bandwidth  $\lambda_1 < \lambda < \lambda_2$  and a given transition  $J \rightarrow J-1$ , we identify a range of cosmological scale factors  $a_1 < a < a_2$  that correspond to our bandwidth. This range of scale factors in turn corresponds to the range of comoving distances  $x_1 < x < x_2$ . However, due to periodic boundary conditions adopted in the simulations, we cannot always model this range of comoving distances directly - if it is large enough, it will correspond to more than one box size. If we simply stack a sufficient number of simulation boxes together, we will get an unphysical result due to periodicity. In order to break this periodicity, we use the approach described in Gnedin & Jaffe (2001): we randomize the neighboring boxes by randomly flipping, transposing, and shifting each of the periodic images of the computational box.

### 3 RESULTS

Figure 1 serves to illustrate the uncertainty of our calculations due to the finite size of the computational box and finite numerical resolution, as measured by the difference between the two simulations A and B. In addition, since both simulations were stopped at  $z = 4$ , a contribution from later redshifts cannot be included. In order to estimate the effect of this contribution, we calculated the CO emission for two cases: no star formation after  $z = 4$ , and constant star formation after  $z = 4$ . The difference between those two cases quantifies the uncertainty due to the finite value for the final redshift of our simulation.

For  $\lambda < 0.3 \text{ cm}$  our calculation is not reliable even in a qualitative sense (to within a factor of 2). At higher wavelengths finite numerical resolution still prevents us from achieving better than about 50% accuracy. More than that, since the star formation rate in our simulations is normalized to the observed value at  $z = 4$ , which is in turn uncertain to at least a factor of two (Nagamine, Cen, & Ostriker 2000; Steidel et al. 1999), our results in general are uncertain to a factor of two to three. However this is quite sufficient for our purpose, which is to emphasize the possibilities rather

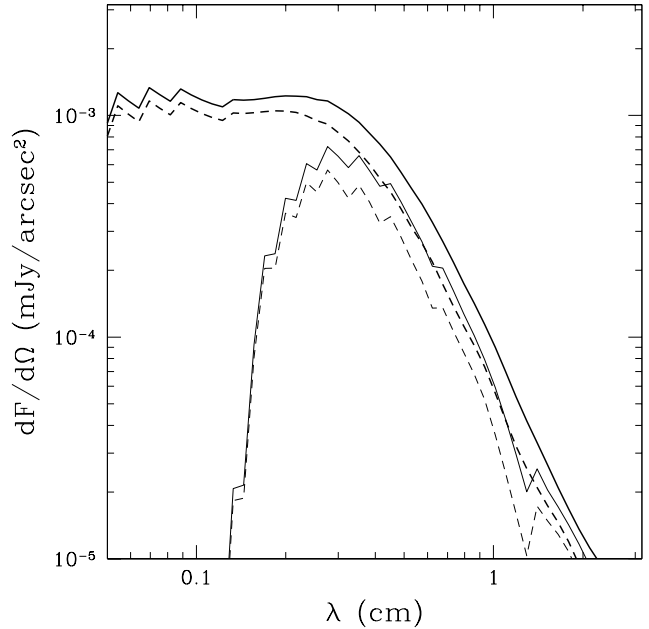
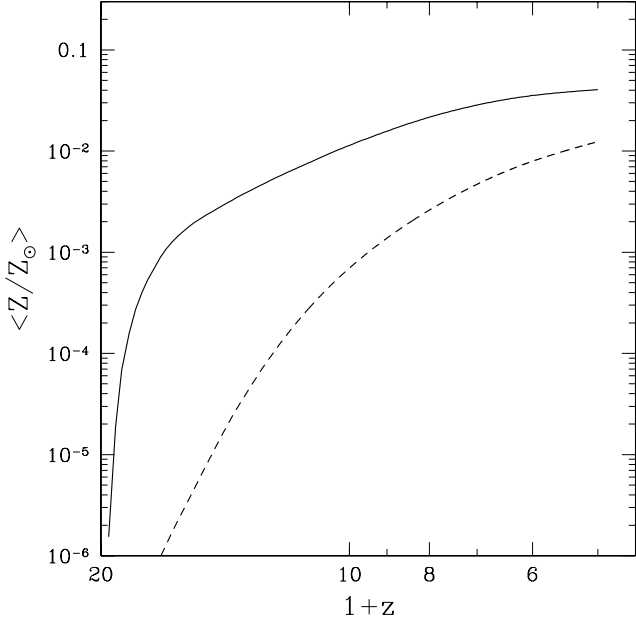


**Figure 1.** The mean CO flux density as a function of wavelength from two simulations: the small simulation box (dashed line) and the large box (solid line), as described in Table 1. Thin lines show the calculation with the star formation rate set to zero after the final redshift of simulation ( $z = 4$ ); bold lines are for the case when the star formation rate is assumed constant for  $z < 4$ . The difference between the two sets of lines is our theoretical uncertainty due to the final size of the simulation box.

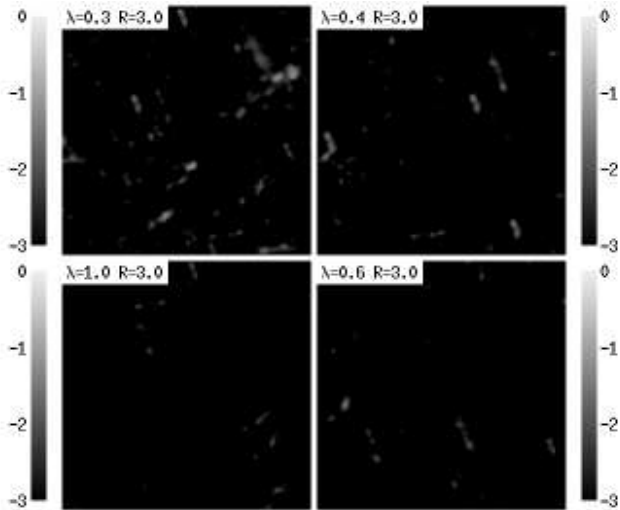
than to make some definite predictions. Because ALMA will not be commissioned until about 2010, theorists have plenty of time to improve upon our calculations and come up with more definitive predictions.

Figure 2 shows the evolution of the mean mass-weighted metallicity of the gas and stars in our large simulation (run A). One can see that stars quickly gain a metallicity of 3% solar by  $z \sim 15$ , and then gain another order of magnitude on average by the end of the simulation at  $z = 4$ . The metallicity of the gas is always lower than stellar, but increases more rapidly. The decrease in stellar metallicities at higher redshifts slightly mitigates the increase in the CO emission due to higher CMB temperature, however it is not sufficient to completely remove the negative K-correction, and thus high redshift star forming galaxies should be considerably brighter than their low redshift counterparts.

In Figure 3 we show our main result: the 4 square degrees of the sky (an image of our computational box) at four different wavelengths. The peak of CO emission corresponds to a broad range of transitions with values in the range of  $J = 5$  to 12 (Silk & Spaans 1997). This means that several epochs correspond to a single observed wavelength:  $\lambda = 0.3 \text{ cm}$  maps redshifts from about 5 to 13,  $\lambda = 0.6 \text{ cm}$  corresponds to redshifts from about 10 to 30, and  $\lambda = 1.0 \text{ cm}$  includes everything from  $z = 20$  to  $z = 50$ . This is somewhat unfortunate, because it means that a simple image at a given wavelength can only provide information about star formation over a range of redshifts. On the other hand, primordial star forming galaxies have relatively narrow velocity ranges, which means that by observing the CO emission in



**Figure 2.** Evolution of the mean mass-weighted metallicity of the gas (dashed line) and stars (solid line).



**Figure 3.** A  $2 \times 2$  degree image of the sky at four different wavelength ( $\lambda = 0.3, 0.4, 0.6,$  and  $1$  cm clockwise from the top left panel, as labeled in the figure) taken with a frequency resolution  $R \equiv \lg(\lambda/\Delta\lambda) = 3$ . Side bars give the correspondence between the color and decimal log of flux density in mJy per square arcsecond.

a narrow wavelength band, it is still possible to disentangle different epochs.

This is illustrated in Figure 4, where we show the same wavelength but at four different spectral resolutions. With a resolution  $\lambda/\Delta\lambda = 10^4$  we can eliminate most of the emission from different redshifts and obtain an image of a single primordial galaxy (lower left panel in Fig. 4). Notice that not only the galaxy itself is measurable by ALMA, but also its satellites - young dwarf spheroidals - are clearly visible in the image. A fortunate circumstance - an enhancement in

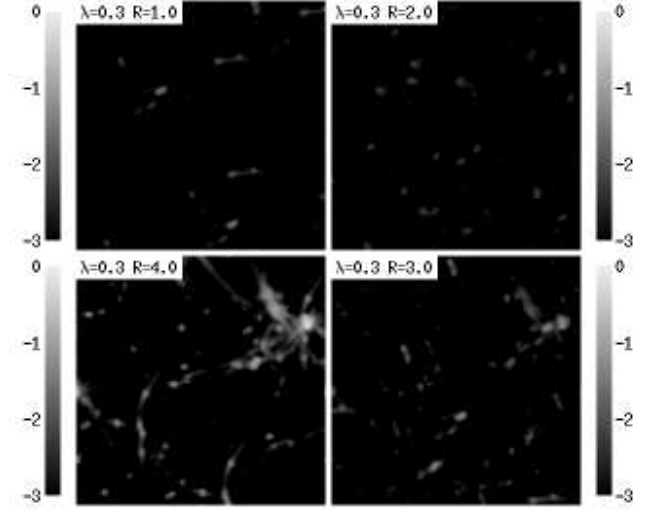


**Figure 4.** A  $2 \times 2$  degree image of the sky at  $\lambda = 0.3$  cm taken with four different wavelength resolutions  $R \equiv \lg(\lambda/\Delta\lambda) = 1, 2, 3,$  and  $4$ , clockwise from the top-left panel (as labeled in the figure). Side bars give the correspondence between the color and decimal log of flux density in mJy per square arcsecond.

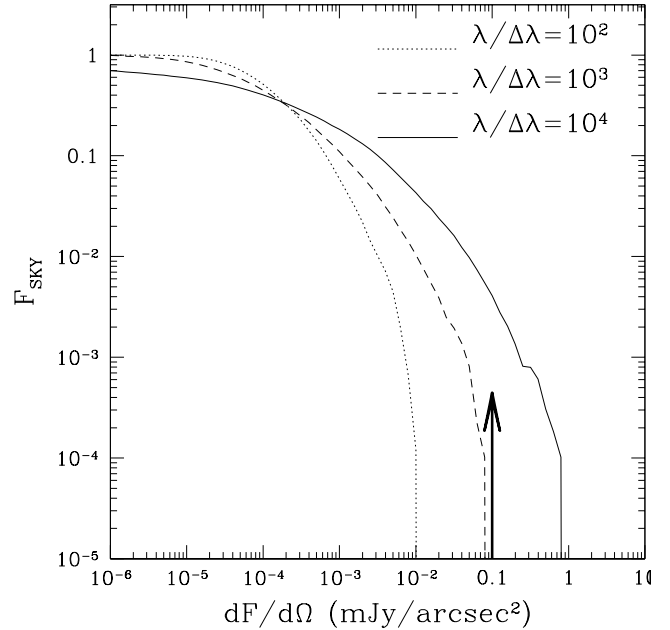


**Figure 5.** Fraction of the sky above a given flux density for three different spectral resolutions at  $\lambda = 0.3$  cm. The black arrow shows ALMA's sensitivity per 1 arcsec<sup>2</sup> pixel for a 100 hour integration (or, equivalently, 1 hour integration on a 10 arcsec<sup>2</sup> source).

population of high  $J$  levels due to higher CMB temperature - may allow ALMA even to see dwarf spheroidals being tidally disrupted in the vicinity of larger galaxies and to map their tidal tails (although this will be a very difficult observation). And, of course, the high redshift picture is much more spectacular than its local equivalents because the merging rate at  $z \sim 10$  is some 500 times higher than in the local universe.

The distribution of flux density on the sky is shown in

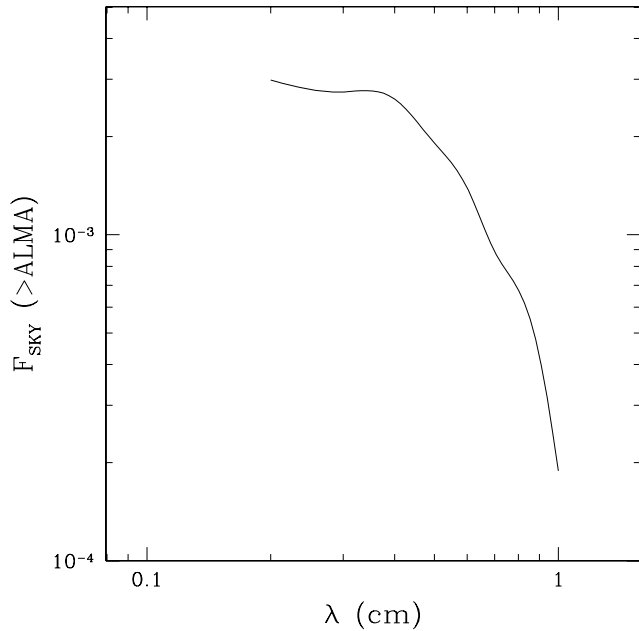


**Figure 6.** Fraction of the sky above the ALMA sensitivity as a function of the wavelength. We only show wavelengths  $\lambda > 0.2$  cm since at shorter wavelengths our calculations become unreliable, as shown by Fig. 1.

Figure 5. We also show a sensitivity limit for ALMA for a typical observation. While ALMA will be just short of measuring typical objects with a spectral resolution of  $10^3$ , at a resolution of  $10^4$  it will be able not only to detect primordial galaxies but also to take their images. High spectral resolution is also required to separate emission from different redshifts, so this mode appears to be the most promising for high redshift observations with ALMA.

Figure 6 summarizes our results by giving the fraction of the sky above the ALMA sensitivity as a function of wavelength. ALMA will have an easy time observing primeval star-forming galaxies at  $z \sim 5 - 10$ , but will not be able to see much beyond that because of the strong decrease in stellar metallicities and star formation rates at higher redshifts. The latter statement is, of course, strongly dependent on the cosmological model - models with large amounts of small scale power will have star formation commencing earlier.

#### 4 CONCLUSIONS

We have demonstrated that future observations with ALMA will be able to detect star-forming primordial galaxies, and even their dwarf spheroidal satellites, in CO emission lines, mostly due to a large negative K-correction. High spectral resolution observations are required to both separate contributions from several objects at different redshifts all emitting at the same wavelength from different rotational levels, and to increase the signal-to-noise. Direct imaging will be possible for galaxies up to redshifts approaching 10. Unfortunately, the expected decrease in the star formation rates and stellar metallicities at higher redshifts will make observations of the era before  $z = 10$  extremely difficult.

A simple possible strategy for these observations might include a shallow large area survey to identify early forming massive galaxies (rare peaks), with subsequent targeted deep observations of their environments. In this case it is possible to observe the same region on the sky at several wavelength bands spaced around several subsequent CO emission lines, in order to get a linear increase in the signal-to-noise.

Broadly speaking, CO emission lines, boosted by higher CMB temperature in the dawn of galaxy formation, will allow millimeter observations with ALMA and other instruments not only to complement observations with the Next Generation Space Telescope (NGST), but, perhaps, to directly compete with the NGST in the race for the highest observable redshifts.

This work was partially supported by National Computational Science Alliance under grant AST-960015N and utilized the SGI/CRAY Origin 2000 array at the National Center for Supercomputing Applications (NCSA).

#### REFERENCES

- Andreani, P., Cimatti, A., Loinard, L., Röttgering, H. 2000, *A&A*, 354, L1
- Barvainis, R., Tacconi, L., Antonucci, R., Alloin, D., Coleman, P. 1994, *Nature*, 371, 586
- Barvainis, R., Alloin, D., Guilloteau, S., Antonucci, R. 1998, *ApJ*, 492, L13
- Blain, A. W., Frayer, D. T., Bock, J. J., Scoville, N. Z. 2000, *MNRAS*, 313, 559
- Combes, F., Maoli, F., Omont, A. 1999, *A&A*, 345, 369
- Downes, D., Neri, R., Wikind, T., Wilner, D. J., Shaver, P. 1999, *ApJ*, 513, L1
- Frayer, D. T., Ivinson, R. J., Scoville, N. Z., Yun, M., Evans, A. S., Smail, I., Blain, A. W., Kneib, J. P. 1998, *ApJ*, 506, L7
- Frayer, D. T., Ivinson, R. J., Scoville, N. Z., Evans, A. S., Yun, M., Smail, I., Barger, A. J., Blain, A. W., Kneib, J. P. 1999, *ApJ*, 514, 13
- Gnedin, N. Y. 2000, *ApJ*, 535, 530
- Gnedin, N. Y., Jaffe, A. H. 2000, *ApJ*, 551, 3
- Guilloteau, S., Omont, A., McMahon, R. G., Cox, P., Petitjean, P. 1997, *A&A*, 328, L1
- Hillenbrand, L. A. 1997, *AJ*, 113, 1733
- Nagamine, K., Cen, R., Ostriker, J. P. 2000, *ApJ*, 541, 25
- Omont, A., Petitjean, P., Guilloteau, S., McMahon, R. G., Solomon, P. M. 1996, *Nat.*, 382, 428
- Papadopoulos, P. P., Röttgering, H. J. A., van der Werf, P. P., Guilloteau, S., Omont, A., van Breugel, W. J. M., Tilanus, R. P. J. 2000, *ApJ*, 528, 626
- Papadopoulos, P., Ivinson, R., Carilli, C., Lewis, G. 2001, *Nat.*, 409, 58
- Sakamoto, S. 1999, *ApJ*, 523, 701
- Scoville, N. Z., Yun, M. S., Windhorst, R. A., Keel, W. C., Armus, L. 1997, *ApJ*, 485, L21
- Solomon, P. M., Downes, D., Radford, S. J. E. 1992, *ApJ*, 398, L29
- Spaans, M. 1996, *A&A*, 307, 271
- Silk J., Spaans, M. 1997, *ApJ*, 488, L79
- Steidel, C. C., Adelberger, K. L., Ciavalisco, M., Dickinson, M., Pettini, M. 1999, *ApJ*, 519, 1